Brazilian Journal
of Chemical
Engineering

ISSN 0104-6632
Printed in Brazil
www.abeq.org.br/bjche

Vol. 32, No. 04, pp. 865 - 873, October - December, 2015
dx.doi.org/10.1590/0104-6632.20150324s00003682

LIQUID FLOW IN IMPELLER SWEPT REGIONS OF BAFFLED AND UNBAFFLED VESSELS WITH A TURBINE-TYPE AGITATOR

M. Yoshida*, H. Ebina, H. Shirosaki, K. Ishioka and K. Oiso

Department of Applied Sciences, Muroran Institute of Technology, 27-1,
Mizumotocho, Muroran 050-8585, Japan.
*E-mail: myoshida@mmm.muroran-it.ac.jp

(Submitted: August 1, 2014 ; Revised: December 17, 2014 ; Accepted: January 20, 2015)

Abstract - Liquid flow in the impeller swept region of vessels with a turbine-type agitator was examined for the flow path between the neighboring blades of the rotating impeller. Visualization of the flow and its measurement were done using particle tracking velocimetry with a camera rotating along with the impeller. Internal liquid flow of the impeller differed when the velocity magnitudes were compared in conditions with and without baffles. Larger circumferential and radial velocities were observed without the baffles and with the baffles, respectively, which was considered to result in the difference of impeller power transmission. Efficiencies produced, based on the flow-head concept, reflected the impeller power characteristics. The turbine-type impeller as an actuator was demonstrated to improve in the flow characteristics with viscous losses increased by the baffles. In terms of impeller efficiencies based on the power consumption, the effect of baffles for the energy was as a decreased transmission and an increased transport.
Keywords: Agitated vessel; Turbine-type agitator; Liquid flow; Impeller swept region; Baffle.

INTRODUCTION

Vessels that are agitated by mechanically rotating impellers are commonly used in industrial applications of chemical processes. When low-viscosity liquids are treated, baffled vessels having a disk turbine impeller with six flat blades are often employed. For such a configuration of the apparatus, knowledge related to the liquid flow within the vessel has been accumulated for utilization in operational and geometrical design (Lee and Yianneskis, 1998). Dynamics of the bulk flow produced by the turbine-type impeller within the vessel were documented by a number of researchers (Yianneskis *et al.*, 1987; Mavros, 2001). Additionally, the characteristics of the liquid flow were elucidated for the region in the vicinity of the impeller, which is essential in the apparatus (Sharp and Adrian, 2001; Yoon *et al.*, 2001). Most of these works confined the observational region to that outside the rotating impeller. Fewer works have examined the liquid flow in the impeller swept region, which is defined as the region swept by the rotating impeller: the region between the neighboring blades of the rotating impeller. Examination of such an internal flow of the impeller as surveyed below enables consideration of the energy conversion upon contact with the impeller blades between the agitator shaft and liquid within the vessel. This provides a guideline for modification and design of blade geometries when the conventional design of the impeller requires improved performance, such as an energy-saving turbine agitator (Rao and Sivashanmugam, 2010), a top shrouded turbine with trapezoidal blades (Singh *et al.*, 2007) and impellers with blades of different shapes and numbers (Ameur and Bouzit, 2012).

*To whom correspondence should be addressed

A survey of earlier studies was made, with emphasis on investigations of the liquid flow in the impeller-swept region of vessels with agitators. Gray (1966) described the theoretical relation between the liquid velocity and the velocity on the periphery of an impeller, using angular momentum theory. By means of that relation, the discharge flow rate was calculated for different designs of impellers. Such a theoretical approach is practically interesting and helpful for performance evaluation considering impeller power characteristics based on the flow-head concept. Unfortunately, he did not refer to the flow through the path between the impeller blades, limiting application to the flow on the impeller periphery, which corresponds to the exit of the flow path. Almost the only literature related to experimental approaches is a report by Takashima and Mochizuki (1971), who conducted tomographic observations and measurements with a camera rotating with an impeller. Although the local flow around the impeller blades was visualized to be characterized by unique models, the data were not analyzed to permit geometrical modification and design for impellers. Computational fluid dynamics (CFD) predictions that have been applied recently to various flow fields can provide detailed information and related knowledge. For the modeling using a grid rotating with an impeller (Ng *et al.*, 1998; Singh *et al.*, 2011), clarification of the internal flow of the impeller is anticipated, but the prediction is regarded as being subject to uncertainty.

Regarding the geometry for operation in low-viscosity liquids, the baffles are usually attached to the vessels to enhance axial mixing by preventing the primary circumferential flow from becoming predominant. Gray (1966) considered the baffle condition and concluded that the baffles have the function of increasing the impeller performance, as evaluated in terms of the discharge flow rate. A baffled vessel has been generally recognized as advantageous for liquid-phase mixing. Consideration should also be given to the effect of baffles on the internal flow of the impeller. Assessing whether the baffles that are external attachments influence the internal flow might be important to conceptualize combined configurations of the impeller and vessel with the baffles, even non-standard configurations (Karcz and Major, 1998; Torre *et al.*, 2007).

To examine the liquid flow in the impeller-swept region of vessels with and without baffles, this study used particle tracking velocimetry with a camera rotating along with an impeller. The internal flow of the turbine type impeller was first measured for its characterization in terms of energy. Additionally, angular momentum theory was used to analyze the experimental data based on the flow-head concept. Geometrical design of the impeller, including attachment of the baffles, in relation to the power characteristics was then discussed in terms of the efficiencies determined from the analytical results for the flow.

EXPERIMENTAL

A schematic diagram of the experimental setup is shown in Figure 1. A fully baffled cylindrical vessel and an unbaffled one with a flat base made of transparent acrylic resin (300 mm inner diameter, D_t) were used. In the former, four vertical baffles with width of $0.1D_t$ were fitted along the internal wall of the vessel, being spaced equally in the circumferential direction. The liquid depth was maintained at D_t: 300 mm. A disk turbine impeller with six flat blades (150 mm diameter, D_i) of standard design was used. It had blade widths of $D_i/4$ and heights of $D_i/5$. The impeller was set at a height of $0.5D_t$ from the vessel bottom. The impeller rotation rate was set to 100 rpm. The impeller power consumption was determined by measuring the torque with strain gauges fitted onto the shaft (Yoshida *et al.*, 2001).

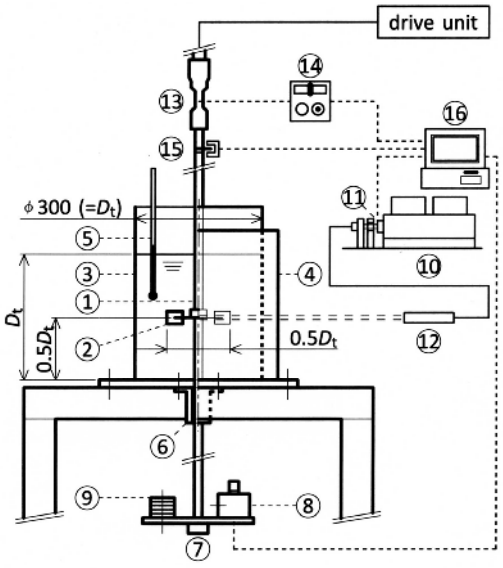

Figure 1: Schematic diagram of the experimental apparatus (dimensions in mm).

Tomographic visualization of the liquid flow was done on the different horizontal planes normal to the impeller shaft, using the particle suspension method. Additionally, the flow velocity was measured using two-dimensional particle tracking velocimetry (PTV). The flow in the direction parallel to the shaft, namely, the axial flow, was out of view for examination. Polystyrene particles (approximately 0.05 mm diameter) were used as tracers. The liquid phase was NaCl solution, with a density equal to that of the tracer particles (1.03 g/cm^3). The liquid viscosity was 1.00 mPa·s. The impeller Reynolds number was 38600, indicating that the bulk liquid flow was turbulent. Images were recorded using a video camera. A 0.5 W laser light sheet adjusted to 2 mm thickness was used for lighting. Lighting was collimated to illuminate the different horizontal planes covering the lower half of the impeller blade. Its height, measured as the distance between the centerline of the impeller blade and that of the light sheet, was varied: 1-17 mm. No examination was run for the upper half of the blade. In subsequent analyses, calculations were made on the assumption of vertical symmetry. The circumferential and radial velocities of liquid flow were examined based on pictures taken with the camera set on a turntable underneath the vessel. The table was attached on the same shaft as that driving the impeller. Details of settings for analysis in PTV incorporating the binary cross-correlation method (Uemura *et al.*, 1990) were described in a previous paper (Yoshida *et al.*, 2007). The coordinate system defined on the horizontal and vertical planes and the test area for measuring the liquid flow velocity are presented in Figure 2.

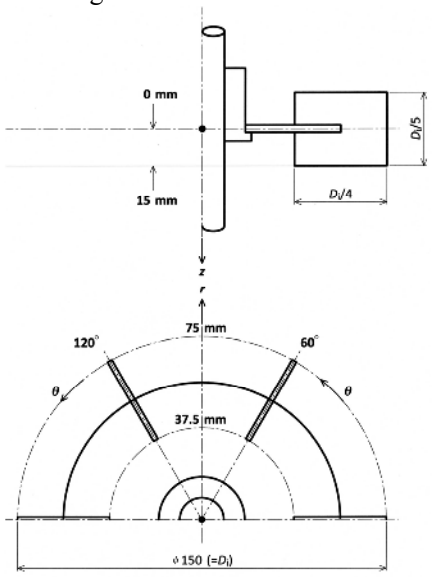

Figure 2: Coordinate system and test area to analyze liquid flow.

Cylindrical coordinates were used: The origin was designated as the intersection between the shaft centerline and the plane including the impeller blade centerline. The circumferential angle was measured in the orientation depicted in Figure 2. After setting the two instantaneous images in series, the liquid flow velocity through a section (2.5 × 2.5 mm = 12.5 × 12.5 pixels) in the test area was determined as the vector based on the difference in position between the tracer particles identified on the composite image and the time between camera frames (1/1000 s). Velocity vectors collected during 40 rotations of the impeller were averaged, being weighted for the distance between the measured point and the section center.

RESULTS AND DISCUSSION

Velocity Profile of the Liquid Flow

Figure 3 (a) depicts typical profiles of the liquid flow velocity when the height measured related to the impeller, the axial distance, *Z*, was varied under the baffled condition. In the figure, the vectors are shown for the velocity relative to that of the impeller rotation. On the horizontal plane including by the midsection of the impeller blade for a representative *Z*=3 mm, a roll vortex was observed around the blade inner edge, as illustrated by Van't Riet and Smith (1973). On its exterior, forced rotation of the liquid between the blades produced outward flows with the centrifugal force. In the front of the blade, the streams run toward the blade and impact onto its surface. In the rear, the streams are practically aligned with the blade, remaining in contact with its surface. Streams from the front and those from the rear were followed to meet in the vicinity of the blade outer edge and to run out by discharge action through the impeller. The flow along the blade surface became weak toward the blade lower edge as *Z* increased. On the horizontal plane including by the lower edge of the impeller blade for a representative *Z*=15 mm, it was inferred that the streams which strike the front surface of the blade ride over the lower edge. This is considered to be an influence of the roll vortex that can grow running over the blade trailing edge from the front to the rear (Van't Riet and Smith, 1973). Comparatively higher velocities were observed on a backward side of the blade on the plane of *Z*=17 mm where the height is just outside of the impeller swept region. This observation implies a flow entering the impeller swept region (Yianneskis and Whitelaw, 1993). Such a flow might

be attributable to the behavior of the trailing vortex. Its core line reportedly continues from that of the roll vortex around the blade inner edge (Van't Riet and Smith, 1973; Yianneskis and Whitelaw, 1993).

Figure 3 (b) depicts typical profiles of the liquid flow velocity under the unbaffled condition. Characteristic streams were observed more or less in common with the baffle conditions. As the figure shows, the relative velocities were lower in most cases than those with the baffles, the liquid flow between the blades approaching the impeller rotation. Additionally, unlike in the case of the baffled condition, a field having locally larger velocities was vanishingly observed on the horizontal planes, including by the lower edge of the impeller blade. The trailing vortex reportedly forms behind the blade for the unbaffled vessel. Its trajectory was similar to that for the baffled vessel (Alcamo *et al.*, 2005). However, the rotation rate in that region might differ according to the baffle conditions. These results suggest that flow behaviors in the impeller-swept region are influenced by the baffles.

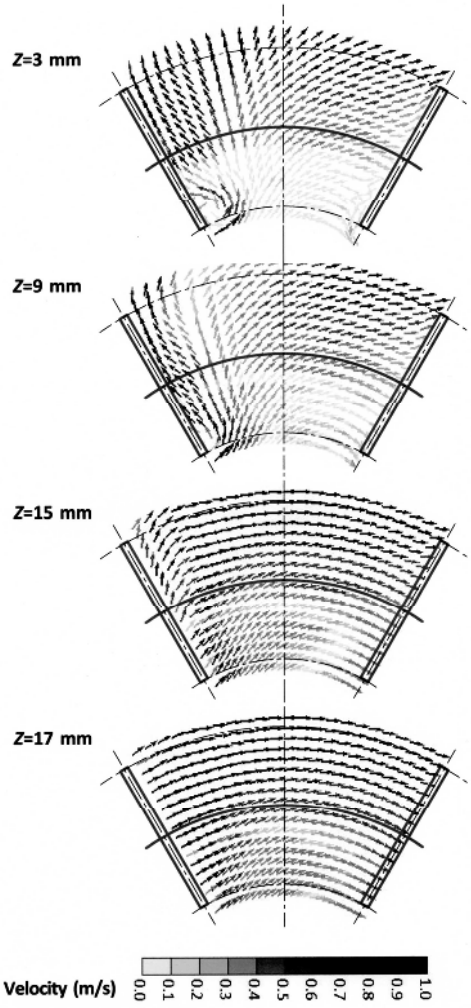

Figure 3 (a): Flow velocity profiles at different heights in the impeller-swept region of the baffled vessel. Rotation orientation is counterclockwise: the surfaces of the right and left blades in the test area respectively correspond to the front side and the rear.

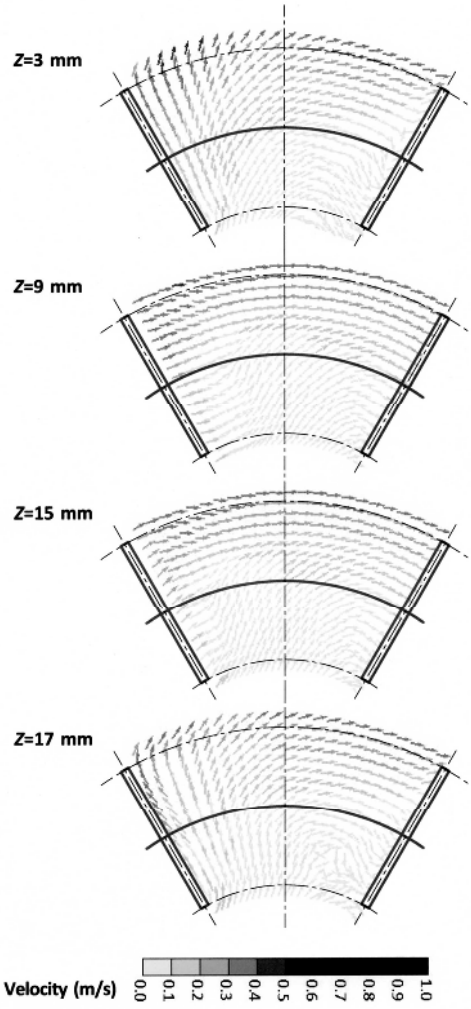

Figure 3 (b): Flow velocity profiles at different heights in the impeller-swept region of the unbaffled vessel. Rotation orientation is counterclockwise: the surfaces of the right and left blades in the test area respectively correspond to the front side and the rear.

Circumferential and Radial Velocities of the Liquid Flow

The vector of the liquid flow velocity has circumferential and radial components: v_θ and v_r. Figure 4 shows the changes of v_θ and v_r with the circumferential angle, Θ, at different axial distances, Zs. At 55 mm of radial distance, R, corresponding to a midstream of the flow path between the blades, v_θ tended to increase in sections near the blade surface (Θ=60 and 120 deg), irrespective of the baffle condition. Concurrently, v_r had a tendency to increase from the front (Θ=60 deg) to the rear (Θ=120 deg) of the blade. For the variation of Z, the differences of v_θ and v_r were found to be larger with the baffles than without the baffles. Downstream of the flow path, as typified by the position of R=75 mm, the dependences of the velocities on Z became larger at the blade rear for both conditions with and without the baffles. A markedly larger dependence was observed under the baffled condition. Attaching the baffle affects the increase of velocity dependence on Z, namely the velocity gradient formed in the axial direction. An increased velocity gradient can enhance the generation of turbulence in the flow and induction of secondary flow. The influence of such a flow behavior, which has been recognized to be a function of the baffle (Nagata *et al.*, 1959a; Nagata *et al.*, 1959b), was reasonably supported through examination of the internal flow of the impeller.

The complicated profile of the liquid flow velocity was coordinated in terms of the circumferential and radial components averaged for the circumferential and axial directions. Figure 5 shows the changes of the average velocities, v_θ and v_r, with the radial distance, R. Independent of the baffle condition, v_θ increased along the flow path between the blades as R increased and leveled off near the path exit (R=75 mm). On the other hand, v_r increased over the entire R range. For the difference dependent on the baffles, it was found that v_θ was larger without the baffles, but v_r exhibited the opposite tendency. These results were interpreted as a difference in energy with the flow-head concept (Edwards *et al.*, 1992; Wu *et al.*, 1997; Srilatha *et al.*, 2008; Fort, 2011). The total head imparted to the liquid on the impeller blade is related to the circumferential velocity. The volumetric flow rate of the liquid passing between the blades is determined by the radial velocity. The head and flow should respectively reflect the intensity and rate of the energy transmitted by the impeller. Thus, although the transmission per liquid mass is advantageous without the baffles, that per time is favorable with the baffles.

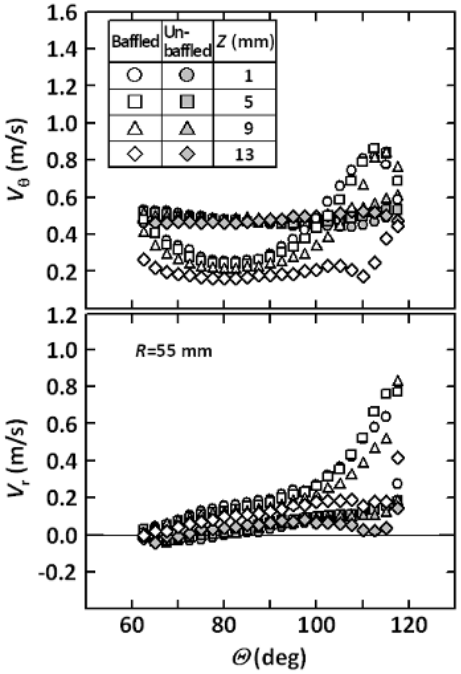

Figure 4 (a): Changes of the circumferential and radial velocities as viewed from the circumferential and axial positions (radial distance, R=55 mm).

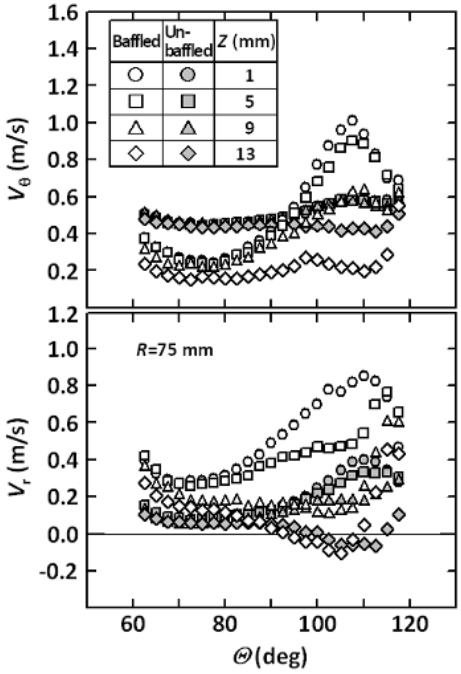

Figure 4 (b): Changes of the circumferential and radial velocities as viewed from the circumferential and axial positions (radial distance, R=75 mm).

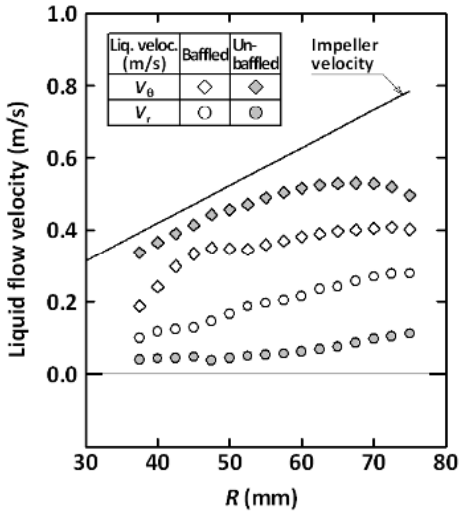

Figure 5: Changes of average flow velocities as viewed from a radial position

Impeller Efficiencies Based on the Flow-Head Concept

The angular momentum theory was applied to analysis of the internal flow of the impeller employing the control surfaces and volume depicted in Figure 6. A modeled flow pattern was assumed in which liquid flows in the control volume across surfaces 1 and 3 and flows out across surface 2. An additional assumption was made that the liquid flows radially and uniformly through the path between the neighboring blades of the rotating impeller. In conjunction with this, the viscous force on the blade surfaces was determined as beyond consideration. The system was simplified further by neglecting the forces on the control surfaces. The related matter was followed by the mechanical balance caused by the action-reaction forces between the blades and liquid. The moment on the shaft fitted with the impeller is given as the temporal rate of change of the angular momentum. Expressing the relation to the circumferential and radial velocities, v_θ and v_r, based on the flow (Q) -head (H) concept,

$$\begin{aligned}\Delta P &= \Delta\{(\rho Q)(gH)\} \\ &= (\rho Q)\cdot\Delta(gH)+\Delta(\rho Q)\cdot(gH) \\ &= (\rho v_r S)\cdot\Delta(uv_\theta)+\Delta(\rho v_r S)\cdot(uv_\theta)\end{aligned} \tag{1}$$

where P is the power transmission of the impeller, S is the area of the surface normal to the r direction, u is the velocity of impeller rotation, that changes depending on r position. ρ is the liquid density and g is the acceleration due to gravity, and they were treated as constant. Equation (1) expresses the power characteristics related to the internal flow of the impeller.

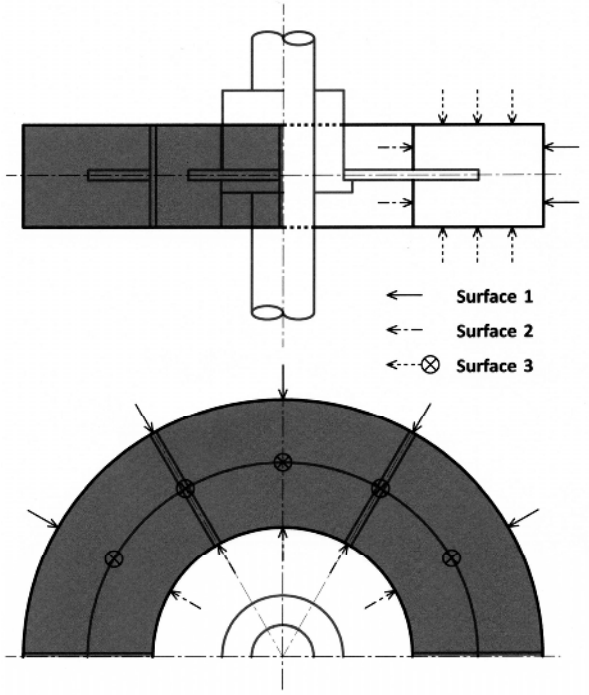

Figure 6: Control surfaces and volume determined in the impeller-swept region

For the flow described above, neglect of the forces on the control surfaces gives a condition that the angular momentum of the liquid inflowing at any r position is equal to that of a liquid at the related position within the rotating impeller. Then, Eq. (1) is reduced to

$$\begin{aligned}\Delta P &= \Delta\{(\rho Q)(gH)\} = (\rho Q)\cdot\Delta(gH) \\ &= (\rho v_r S)\cdot\Delta(uv_\theta)\end{aligned} \tag{2}$$

Integration of Eq. (2) from the entrance of the flow path to its exit yields the following equation:

$$\begin{aligned}P &= \sum\{(\rho Q)\cdot\Delta(gH)\} \\ &= \sum\left[\left\{\frac{(\rho v_r S)_{i+1}+(\rho v_r S)_i}{2}\right\}\{(uv_\theta)_{i+1}-(uv_\theta)_i\}\right]\end{aligned} \tag{3}$$

In Eq. (3), v_θ was regarded as u from the assumption of radial and uniform flow. Additionally, the flow was considered as having v_r equal to v_θ, namely, u. Calculation of P_m was made using u that modeled the

flow. Concurrently, $(gH)_m$ and $(\rho Q)_m$ for the modeled flow were determined as follows.

$$(gH)_m = {u_2}^2 - {u_1}^2 \tag{4}$$

$$(\rho Q)_m = \frac{P_m}{(gH)_m} \tag{5}$$

Suffixes 1 and 2, respectively, denote control surfaces 1 and 2, corresponding to the entrance and exit of the flow path. In the actual flow, v_θ and v_r are generally not equal to u. Calculation of P_as from Eq. (3) was made using v_θs and v_rs measured under conditions with and without baffles. $(gH)_a$ and $(\rho Q)_a$ for the actual flow were determined as for the modeled flow.

$$(gH)_a = (uv_\theta)_2 - (uv_\theta)_1 \tag{6}$$

$$(\rho Q)_a = \frac{P_a}{(gH)_a} \tag{7}$$

The analytical results are summarized in Table 1 as quantities for the actual flow relative to those for the modeled flow. These ratios were perceived to be efficiencies expressing the differences between the actual and modeled flows in terms of the flow and head. The differences depending on the baffle condition, as shown in Figure 5, are indicated by the ratios. Thus, the head characteristic related to the circumferential velocity was efficient without the baffles, but the flow determined by the radial velocity was efficient with the baffles. The increased flow rate under the baffle condition is attributable mainly to the larger inflow across surface 3. The axial inflow can disturb the flow along the blade surface in the path. It seems to follow that the head characteristic was decreased. Roughly assessing the efficiency for a turbine type impeller of standard design, as used in this work, the respective flow and head efficiencies were about 10-30 % and 50 %. Results show that the power efficiency was about 10 %, which implies that 10 % of the total in the impeller blades works for the energy transmission. For modification and design of the blade geometries of the turbine-type impeller, a guideline should be proposed so that improvement of the flow efficiency is considerable. Then, introduction of these parameters based on the flow-head concept might provide sound ideas for the design of improved impellers.

Table 1: Impeller efficiencies calculated based on analysis of the internal liquid flow.

Baffle	P_a/P_m (-)	$(gH)_a/(gH)_m$ (-)	$(\rho Q)_a/(\rho Q)_m$ (-)	E_1 (-)	E_2 (-)
with	0.146	0.523	0.279	0.266	0.0679
without	0.0455	0.556	0.0817	0.346	0.0184

Impeller Efficiencies Based on the Power Consumption

The power transmission of the impeller, P, as calculated from Eq. (3) for the actual flow, was compared with the power consumption of the impeller, P'. The ratio, P/P', which was added to Table 1 as E_1, was regarded as another efficiency considering viscous losses in the internal flow of the impeller. E_1 without the baffles was larger than that with the baffles. This difference seems to reflect the difference of the velocity gradient formed in the flow. The larger the gradient is, the larger the viscous loss is with increased turbulence, resulting in a decreased E_1. The larger E_1 without the baffles is considered to result from the smaller velocity gradient formed in the axial direction, as shown in Figure 4. Conceptually, E_1 is identical to the hydraulic efficiency defined by Fort (2011). This parameter expresses the portion of the impeller power input that is dissipated entirely within the vessel except for the impeller swept region. Such an impeller power output is used effectively outside the impeller swept region. The efficiency, E_1, is expected to be important in design, conditioning the energy dissipations in the internal and external flows of the impeller. Moreover, a higher E_1 value is not always desirable. For operations with mixing and dispersion of one phase in another phase, the shear action in flows produced by an impeller is enhanced for the impeller having a lower E_1 value. It is to be noted that E_1 is an indicator for the impeller design with energy considerations.

Hitherto, some efficiencies of the impeller have been proposed to assess the power characteristics (Nienow, 1997; Fentiman *et al.*, 1998; Wu *et al.*, 2006; Fort, 2011). A parameter incorporating the impeller power number, N_p, and discharge flow number, N_d, is possibly employed.

$$E_2 = \frac{{N_d}^3}{N_p} \tag{8}$$

Table 1 includes E_2 values. Comparison of the effect of baffles in terms of the two efficiencies, E_1 and E_2, leads to a conflicting assessment, with a larger E_1

without the baffles and larger E_2 with the baffles. Because these efficiencies are based on the impeller power consumption, the difference in assessments is attributable to the different quantities expressed by the numerator terms in the definition equations. In E_1, the impeller power transmission is the factor considered. E_2 considers the kinetic energy of the liquid discharged by the impeller. Therefore, E_1 represents the efficiency of the energy transmission and E_2 represents the efficiency integrating the energy transmission, conversion and transport within the vessel. The effect of baffles on the impeller power characteristics is evaluated as follows: although the baffles make the impeller less efficient for the energy transmission, the overall efficiency is improved within the baffled vessel, being caused by efficient energy transport. Use of the efficiency presented here, E_1, in addition to the existing one, E_2, is useful for consideration of the energy of the liquid flow within the vessel. It enables a fundamental assessment of the impeller power characteristics.

CONCLUSIONS

For baffled and unbaffled vessels with the turbine-type agitator, we experimentally investigated the liquid flow in the impeller-swept region, considering power characteristics of the impeller. The liquid flow velocity profiles on the horizontal planes including the impeller of the respective vessels were more or less similar in their flow pattern, but they differed in the velocity magnitude between the baffle conditions. The circumferential and radial components into which the velocity vectors were divided were compared in their magnitudes. Overall, the circumferential and radial velocities were typically higher without the baffles and with the baffles, respectively. Energy considerations based on the flow-head concept explained these tendencies because the baffle was effective not for specific energy transmission but temporally. Collaterally, efficiencies related to the impeller power characteristics were defined. Assessment in terms of the efficiencies demonstrated for the turbine-type impeller that an improvement was desirable in the flow characteristics rather than the head. Finally, the impeller efficiencies based on the power consumption, E_1 and E_2, were discussed. In the impeller-swept region where the energy transmission is performed, the baffles were suggested to increase viscous losses, since E_1 decreased by about 23%. On the other hand, the baffles were found to improve the overall liquid flow within the vessel, increasing E_2 up to about 3.7 times.

NOMENCLATURE

D_i	impeller diameter (mm)
D_t	vessel diameter (mm)
E_1	impeller efficiency defined as P/P' (-)
E_2	impeller efficiency defined by Eq. (8) (-)
g	acceleration due to gravity (m/s^2)
H	head in flow (m)
N_p	impeller power number (-)
N_q	discharge flow number (-)
P	impeller power transmission (W)
P'	impeller power consumption (W)
Q	volumetric flow rate (m^3/s)
R	radial distance (mm)
r	radial direction in the coordinate system as shown in Figure 2
S	area of the surface normal to the radial direction (m^2)
u	velocity of impeller rotation (m/s)
v_r	radial velocity component of liquid flow (m/s)
v_θ	circumferential velocity component of liquid flow (m/s)
Z	axial distance (mm)
z	axial direction in the coordinate system as shown in Figure 2

Greek Letters

Θ	circumferential angle (deg)
θ	circumferential direction in the coordinate system as shown in Figure 2
ρ	density of liquid (kg/m^3)

REFERENCES

Alcamo, R., Micale, G., Grisafi, F., Brucato, A., Ciofalo, M., Large-eddy simulation of turbulent flow in an unbaffled stirred tank driven by a Rushton turbine. Chem. Eng. Sci., 60, 2303-2316 (2005).

Ameur, H., Bouzit, M., Mixing in shear thinning fluids. Braz. J. Chem. Eng., 29, 349-358 (2012).

Edwards, M. F., Baker, M. R., Godfrey, J. C., Mixing of Liquids in Stirred Tanks. Edwards, M. F., Nienow, A. W. Ed., Mixing in the Process Industries, pp. 137-158, Butterworth- Heinemann, Oxford (1992).

Fentiman, N. J., St Hill, N., Lee, K. C., Paul, G. R., Yianneskis, M., A novel profiled blade impeller for homogenization of miscible liquids in stirred vessels. Chem. Eng. Res. Des., 76, 835-842 (1998).

Fort, I., On hydraulic efficiency of pitched blade

impellers. Chem. Eng. Res. Des., 89, 611-615 (2011).

Gray, J. B., Flow Patterns, Fluid Velocities, and Mixing in Agitated Vessels. Uhl, V. W., Gray, J. B. Ed., Mixing, Theory and Practice 1, pp. 179-278, Academic Press, New York and London (1966).

Karcz, J., Major, M., An effect of a baffle length on the power consumption in an agitated vessel. Chem. Eng. Process., 37, 249-256 (1998).

Lee, K. C., Yianneskis, M., Turbulence properties of the impeller stream of a Rushton turbine. AIChE J., 44, 13-24 (1998).

Mavros, P., Flow visualization in stirred vessels, A review of experimental techniques. Chem. Eng. Res. Des., 79, 113-127 (2001).

Nagata, S., Yamamoto, K., Ujihara, M., Flow patterns of liquid in a cylindrical mixing vessel without baffles. Kagaku Kogaku, 23, 130-137 (1959a).

Nagata, S., Yamamoto, K., Hashimoto, K., Naruse, Y., Flow patterns of liquid in a cylindrical mixing vessel with baffles. Kagaku Kogaku, 23, 595-602 (1959b).

Ng, K., Fentiman, N. J., Lee, K. C., Yianneskis, M., Assessment of slidingmesh CFD predictions and LDA measurements of the flow in a tank stirred by a Rushton impeller. Chem. Eng. Res. Des., 76, 737-747 (1998).

Nienow, A. W., On impeller circulation and mixing effectiveness in the turbulent flow regime. Chem. Eng. Sci., 52, 2557-2565 (1997).

Rao, D. A., Sivashanmugam, P., Experimental and CFD simulation studies on power consumption in mixing using energy saving turbine agitator. J. Ind. Eng. Chem., 16, 157-161 (2010).

Sharp, K. V., Adrian, R. J., PIV Study of small-scale flow structure around a Rushton turbine. AIChE J., 47, 766-778 (2001).

Singh, K. K., Mahajani, S. M., Shenoy, K. T., Patwardhan, A. W., Ghosh, S. K., CFD modeling of pilot-scale pump-mixer, Single-phase head and power characteristics. Chem. Eng. Sci., 62, 1308-1322 (2007).

Singh, H., Fletcher, D. F., Nijdam, J. J., An assessment of different turbulence models for predicting flow in a baffled tank stirred with a Rushton turbine. Chem. Eng. Sci., 66, 5976-5988 (2011).

Srilatha, C., Savant, A. R., Patwardhan, A. W., Ghosh, S. K., Head-flow characteristics of pump-mix mixers. Chem. Eng. Process., 47, 1678-1692 (2008).

Takashima, I., Mochizuki, M., Tomographic observations of the flow around agitator impeller. J. Chem. Eng. Japan, 4, 66-72 (1971).

Torre, J. P., Fletcher, D. F., Lasuye, T., Xuereb, C., Single and multiphase CFD approaches for modelling partially baffled stirred vessels: Comparison of experimental data with numerical predictions. Chem. Eng. Sci., 62, 6246-6262 (2007).

Uemura, T., Yamamoto, F., Sachikawa, M., High-speed image analysis algorithm for particle tracking velocimetry. Trans. Visualization Soc. Japan, 10, 196-202 (1990).

Van't Riet, K., Smith, J. M., The behaviour of gas-liquid mixtures near Rushton turbine blades. Chem. Eng. Sci., 28, 1031-1037 (1973).

Wu, J., Pullum, L., Yunken, R., Welsh, M. C., Rapid diagnosis of flow separation around an axial impeller in a mixing vessel. Exp. Fluids, 22, 519-522 (1997).

Wu, J., Graham, L. J., Nguyen, B., Mehidi, M. N. N., Energy efficiency study on axial flow impellers. Chem. Eng. Process., 45, 625-632 (2006).

Yianneskis, M., Popiolek, Z., Whitelaw, J. H., An experimental study of the steady and unsteady flow characteristics of stirred reactors. J. Fluid Mech., 175, 537-555 (1987).

Yianneskis, M., Whitelaw, J. H., On the structure of the trailing vortices around Rushton turbine blades. Chem. Eng. Res. Des., 71, 543-550 (1993).

Yoon, H. S., Sharp, K. V., Hill, D. F., Adrian, R. J., Balachandar, S., Ha, M. Y., Kar, K., Integrated experimental and computational approach to simulation of flow in a stirred tank. Chem. Eng. Sci., 56, 6635-6649 (2001).

Yoshida, M., Ito, A., Yamagiwa, K., Ohkawa, A., Abe, M., Tezura, S., Shimazaki, M., Power characteristics of unsteadily forward-reverse rotating impellers in an unbaffled aerated agitated vessel. J. Chem. Technol. Biotechnol., 76, 383-392 (2001).

Yoshida, M., Shigeyama, M., Hiura, T., Yamagiwa, K., Ohkawa, A., Tezura, S., Liquid flow in impeller region of an unbaffled agitated vessel with unsteadily forward-reverse rotating impeller. Chem. Eng. Comms., 194, 1229-1240 (2007).